Low-Order Models for Turbulent Flows over Complex Walls

Mitul Luhar

Department of Aerospace and Mechanical Engineering
University of Southern California
Los Angeles, CA 90089
luhar@usc.edu

ABSTRACT

Porous and patterned surfaces appear in many turbulent flows of engineering and scientific interest. Yet, there are few computationally efficient models that can predict how such complex walls alter spectral and structural features of the turbulent flow field. The present effort seeks to address this limitation by extending the resolvent formulation proposed by McKeon & Sharma (2010). Under the resolvent formulation, the turbulent velocity field is expressed as a linear superposition of propagating modes, identified via a gain-based decomposition of the governing Navier-Stokes equations. To account for porous and patterned surfaces, the resolvent framework is extended to the volume-averaged Navier-Stokes equations, such that the effect of the complex substrate appears explicitly as an additional body force: a generalized version of Darcy's law. The permeability is infinite within the fluid domain so that the body force is zero. Solid domains are modeled as regions with (near) zero permeability. For a complex porous substrate, the permeability depends on the specific microstructure i.e. the size, distribution, and alignment of pores. Preliminary results show that a gain-based decomposition of the volume-averaged Navier-Stokes equations is able to reproduce many key observations from previous simulations of flow over streamwise-constant riblets (Garcia-Mayoral & Jimenez, 2011) as well as homogeneous porous media (Breugem *et al.*, 2006).

INTRODUCTION

Many turbulent flows in nature and engineering are characterized by the presence of complex walls (e.g. porous, rough, or patterned) that can substantially alter the near-wall turbulence. For example, in flows over porous media and vegetation canopies, the streaks and streamwise vortices prevalent in smooth-walled flows are often replaced by structures resembling Kelvin-Helmholtz vortices (Breugem *et al.*, 2006; Ghisalberti, 2009). In recent years, similar large-scale structures have also been observed over riblets (Garcia-Mayoral & Jimenez, 2011; García-Mayoral & Jiménez, 2011), modifying the traditional view that the deterioration of riblet performance with increasing riblet spacing is due to the lodging of near-wall streamwise vortices within the riblet grooves. While stability analyses can reproduce some of these observations, they are limited in their ability to generate low-order models for spectra and coherent structure in fully turbulent flows. The present effort seeks to address this limitation by extending the resolvent formulation proposed by McKeon & Sharma (2010) to account for complex walls.

MODELING APPROACH

Resolvent Formulation

The resolvent formulation decomposes the full turbulent velocity field into a limited set of highly-amplified traveling waves, or modes, identified *directly* from the governing NSE. Specifically, the formulation interprets the Fourier-transformed NSE as a forcing-response system with nonlinear feedback. For each wavenumber-frequency triplet $\mathbf{k} = (\kappa_x, \kappa_z, \omega)$, corresponding to a traveling wave of specified streamwise wavelength ($\lambda_x = 2\pi/\kappa_x$), spanwise wavelength ($\lambda_z = 2\pi/\kappa_z$), and frequency, the nonlinear terms, $\mathbf{f_k} = (-\mathbf{u}\cdot\nabla\mathbf{u})_\mathbf{k}$, are interpreted as the forcing that gives rise to a velocity, $\mathbf{u_k}$, and pressure, $p_\mathbf{k}$, field in response. The transfer function that maps the nonlinear forcing to the velocity and pressure response is the resolvent operator $\mathbf{H_k}$. With this forcing-response interpretation, the Fourier-transformed NSE can be expressed compactly as:

$$\begin{bmatrix}\mathbf{u_k}\\ p_\mathbf{k}\end{bmatrix} = \left(-i\omega\begin{bmatrix}\mathbf{I} & \\ & 0\end{bmatrix} - \begin{bmatrix}\mathbf{L_k} & -\nabla_\mathbf{k}\\ \nabla_\mathbf{k}^T & 0\end{bmatrix}\right)^{-1}\begin{bmatrix}\mathbf{I}\\ 0\end{bmatrix}\mathbf{f_k} = \mathbf{H_k}\mathbf{f_k} \quad (1)$$

where $\mathbf{u_k}$, $p_\mathbf{k}$, and $\mathbf{f_k}$ represent the complex Fourier coefficients that vary in the wall-normal (y) direction, and the common complex exponential $\exp i(\kappa_x x + \kappa_z z - \omega t)$ has been omitted from both sides. $\mathbf{L_k}$ is the linearized Navier-Stokes operator, which requires knowledge of the mean velocity profile, $U(y)$. The first row of the expression inside the parenthesis on the right-hand side represents the momentum equations, while the second row enforces continuity $\nabla\cdot\mathbf{u} = 0$. Keep in mind that the formulation presented above is only valid for fully developed channel or pipe flows, which can be considered homogeneous in the streamwise and spanwise (or azimuthal) directions and stationary in time. However, it can also approximate boundary layer flows, assuming slow variation in the streamwise direction.

Even though the resolvent framework interprets the NSE as a linear forcing-response system, this does not mean that the equations have been linearized. A complete description of the flow still requires knowledge of how the velocity responses interact to generate the nonlinear forcing $\mathbf{f_k}$. The resolvent operator can be considered a filter that determines how this forcing is translated into velocity and pressure responses across spectral space. A major contribution of the resolvent framework lies in the finding that the transfer function $\mathbf{H_k}$ tends to be low-rank at wavenumber-frequency combinations energetic in natural flows (Moarref *et al.*, 2013). In other words, $\mathbf{H_k}$ is a very directional amplifier: only a few forcing functions lead to highly amplified velocity responses. As a result, the forcing-response relationship is well approximated by the first modes calculated under a simple singular value decomposition (SVD) of the resolvent (McKeon & Sharma, 2010):

$$\mathbf{H_k} = \sum_m \psi_m\sigma_m\phi_m^* \approx \psi_1\sigma_1\phi_1^*. \quad (2)$$

Physically, this means the first response mode (left singular vector, ψ_1) is so highly amplified that it is expected to dominate the flow field at that wavenumber-frequency combination, as long as some forcing exists in the direction of the first forcing mode (right singular vector, ϕ_1). The first singular value σ_1 represents the degree of amplification in an L^2 energy sense. Previous studies have shown

that this rank-1 approximation reproduces key features of wall-bounded turbulent flows (Moarref *et al.*, 2013; Sharma & McKeon, 2013; Luhar *et al.*, 2014*a*) with minimal computation and also accounts for the effects of passive and active control (Luhar *et al.*, 2014*b*, 2015). This rank-1 approximation also forms the basis of the low-order modeling framework described below.

Volume Penalization

To account for porous and patterned surfaces, the resolvent framework is extended to the volume-averaged NSE, such that the effect of the complex substrate appears explicitly as an additional body force (Khadra *et al.*, 2000; Breugem *et al.*, 2006):

$$\frac{\partial \mathbf{u}}{\partial t} + \frac{1}{\varepsilon}\nabla\cdot(\varepsilon\mathbf{u}\mathbf{u}) = -\nabla p + \frac{1}{\varepsilon Re_\tau}\nabla^2\varepsilon\mathbf{u} - \frac{\mathbf{K}^{-1}}{Re_\tau Da}\varepsilon\mathbf{u}. \qquad (3)$$

In Eq. 3, ε is the porosity, $Re_\tau = u_\tau h/\nu$ is the friction Reynolds number where u_τ is the friction velocity and h is the channel half-height (or boundary layer thickness), $Da = K_0/h^2$ is the Darcy number with K_0 being a representative permeability, and $\mathbf{K}$ is the permeability tensor normalized by K_0.

Within the fluid domain, the porosity is $\varepsilon = 1$ and the permeability tensor is isotropic, $\mathbf{K} = K\mathbf{I}$, with $K = K_f \to \infty$. In other words, the body force term is zero and Eq. 3 reduces to the NSE. Solid domains (e.g. riblets) are modeled as homogeneous, isotropic porous media with porosity $\varepsilon \approx 1$ but negligible permeability, $\mathbf{K} = K_s\mathbf{I}$ with $K_s \to 0$. In other words, the body force is maximum in the solid domain such that the velocity is driven to $|\mathbf{u}| \to 0$. For a complex porous medium, $\mathbf{K}$ depends on the specific microstructure: the size and alignment of pores.

Note that the form and appearance of the extra permeability term in Eq. 3 has been justified rigorously for flows through porous media using homogenization methods (Ochoa-Tapia & Whitaker, 1995*a*,*b*). The assumption that a solid can be effectively modeled as a porous medium with negligible permeability is admittedly ad hoc. However, this assumption has been shown to converge to the no slip boundary condition as $K_s \to 0$. Further details on the mathematical justification and formal convergence properties of this volume-penalizing formulation for solid domains can be found in Angot *et al.* (1999) and Khadra *et al.* (2000).

For the current effort, the key advantage of volume penalization is that it enables an extension of the resolvent analysis to arbitrarily complex wall properties and geometries while maintaining the linearity of the forcing-response transfer function and the convenience of working in Fourier space. In other words, since *any* complex patterned or porous substrate can be modeled as a spatially varying permeability, the effect of the surface has a well-defined spectral representation involving the Fourier components of $\mathbf{K}$. Eq. 3 can be Fourier-transformed in the streamwise direction, spanwise direction, and time, and expressed as:

$$\begin{bmatrix}\mathbf{u}_{\tilde{\mathbf{k}}}\\ p_{\tilde{\mathbf{k}}}\end{bmatrix} = \left(-i\omega\begin{bmatrix}\mathbf{I} & \\ & 0\end{bmatrix} - \begin{bmatrix}\mathbf{L}_{\tilde{\mathbf{k}}} - \left(\frac{\mathbf{K}^{-1}\varepsilon}{Re_\tau Da}\right)_{\tilde{\mathbf{k}}} & -\nabla_{\tilde{\mathbf{k}}}\\ \nabla^T_{\tilde{\mathbf{k}}}\varepsilon & 0\end{bmatrix}\right)^{-1} \begin{bmatrix}-(\frac{1}{\varepsilon}\nabla\cdot\varepsilon\mathbf{u}\mathbf{u})_{\tilde{\mathbf{k}}}\\ 0\end{bmatrix}, \qquad (4)$$

where the inverted operator on the right-hand side is the modified resolvent, accounting for the new mean velocity profile as well as the complex wall.

For a porous medium that is homogeneous in the streamwise and spanwise directions, the mean velocity profile and the permeability tensor are constant in x and z, which means that the resolvent analysis can proceed as before on a mode-by-mode basis. However, for a spatially-varying complex wall, the mean velocity profile and the permeability tensor also vary in space, i.e. their Fourier representation may involve multiple, (κ_x, κ_z) combinations. In this case, Eq. 4 represents a coupled system of interacting Fourier modes ($\tilde{\mathbf{k}}$).

Numerical Approach

This paper considers (i) the effect of streamwise-constant rectangular riblets at $Re_\tau = 180$ (after Garcia-Mayoral & Jimenez, 2011) and (ii) a channel that is partially filled with a porous medium with $\varepsilon = 0.95$ and $Da = 1.9\times10^{-4}$ at $Re^p_\tau = 498$, defined using the friction velocity at the porous interface (after Breugem *et al.*, 2006). In both cases, the numerical implementation involves a pseudospectral discretization in the wall-normal direction on $N \geq 100$ Chebyshev collocation points over the channel half-height.

To account for the effect of riblets with spacing s and varying cross-section, the permeability is modeled as spanwise-periodic. In the solid domain, corresponding to the local riblet width $b(y)$, the permeability goes to zero (actually, 10^{-8}). In the fluid domain, the permeability is infinite, such that $K^{-1} = 0$. This periodic train of permeability 'pulses' has a well-defined Fourier representation involving harmonics of the spanwise wavenumber $\kappa_s = 2\pi/s$:

$$\mathbf{K}^{-1} = K^{-1}\mathbf{I} = \sum_{n=-\infty}^{\infty} a_n(y)\exp(in\kappa_s z)\mathbf{I}, \qquad (5)$$

where the Fourier coefficients $a_n(y)$ depend on the height and shape of the riblets. Similarly, the modified mean velocity profile over the riblets also includes harmonics of the spanwise wavenumber κ_s. For this spatially-varying permeability, Eq. 4 represents a coupled system of Fourier components with wavenumber-frequency combinations

$$\tilde{\mathbf{k}} = (\kappa_x, \kappa_z + \sum_{n=-\infty}^{\infty} n\kappa_s, \omega). \qquad (6)$$

In principle, the analysis can proceed as before with for this coupled system, truncated numerically to $\pm N_H$ harmonics of κ_s. However, the size of the resolvent operator becomes $4N(2N_H+1)\times 4N(2N_H+1)$ in this case. For reasonable choices of N and N_H ($N = 100$ and $N_H = 12$ led to convergence to $O(10^{-2})$), this makes matrix inversion and the SVD computationally expensive for low-order modeling purposes.

To make the computation for riblets more tractable, a two-step procedure is employed. In the first step, the resolvent operator is computed without accounting for the presence of the substrate or additional harmonics in the mean velocity profile. An SVD is used to identify the most amplified forcing and response modes for this simplified resolvent operator. In the second step, the most amplified response mode is corrected to account for interactions with additional harmonics in the mean profile and the complex substrate (i.e. to enforce the boundary conditions), such that Eq. 4 is satisfied. Essentially, this second step amounts to solving a coupled system of linear equations for the rank-1 response mode and the additional velocity harmonics introduced by interactions with spatially-varying $\mathbf{K}$. Depending on the exact spectral features of $\mathbf{K}$, this modification of the rank-1 response can result in the mode being further amplified, or energy being transferred to other wavenumber-frequency combinations.

Note that construction of the resolvent operator also requires mean velocity profiles. For the porous medium, the model predictions utilize the mean velocity profile obtained in DNS (Breugem

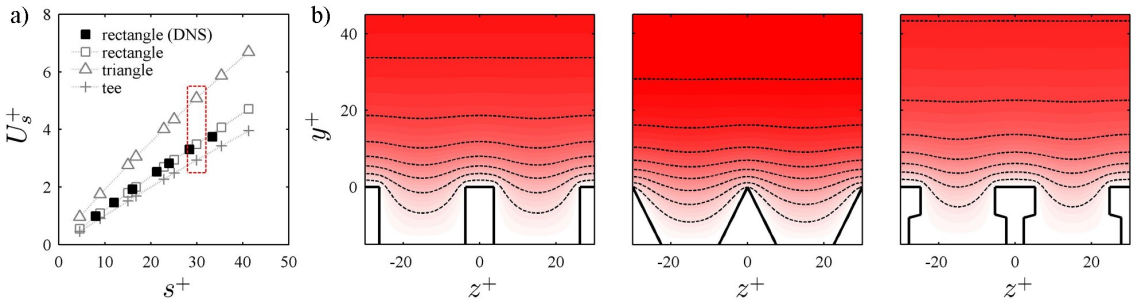

Figure 1. Mean flow predictions for riblets. (a) The predicted slip velocity at the riblet tips as a function of riblet spacing s^+ for three different riblet morphologies; DNS data from (Garcia-Mayoral & Jimenez, 2011). In all cases, riblet height is $0.5s^+$. (b) Mean streamwise velocity for three different cases identified in (a) by the red box. The dashed contour lines show increments of $2u_\tau$.

et al., 2006). For the riblets, the mean profile is computed using Eq. 4, with an eddy viscosity formulation for the region above the riblets (Reynolds & Tiederman, 1967). The flow within the riblet grooves is assumed to remain laminar. Despite these simplifications, Fig. 1 shows that predicted slip velocity at the top of the riblets agrees well with DNS results for rectangular cross-sections. To showcase the versatility of volume penalization, mean velocity predictions are also generated for triangular and T-shaped riblets. As expected intuitively, the slip velocity is higher over triangular riblets and lower for T-shaped riblets.

RESULTS

The potential of the volume-penalized resolvent framework is demonstrated in Figs. 2-4, which compare model predictions for spectra and flow structure with previous DNS for turbulent channel flow over riblets and porous media.

Riblets

Fig. 2 compares model predictions for velocity and Reynolds' stress spectra with DNS results above rectangular riblets with spacing $s^+ = 28$, which *increase* skin friction (Garcia-Mayoral & Jimenez, 2011). These predictions for the premultiplied wavenumber spectra assume *broadband forcing*. That is, the nonlinear forcing is assumed to be in the direction of the most dangerous forcing mode ϕ_1 at all wavenumber frequency combinations. The resulting velocity and pressure fields are then numerically integrated over frequency ω. These spectra are computed for wavelengths ranging from $(\lambda_x^+, \lambda_z^+) \approx 10$ to $(\lambda_x^+, \lambda_z^+) \approx 10^3$, and frequencies corresponding to propagation speeds $c^+ = \omega^+/\kappa_x^+$ ranging from 0 to the maximum value of U^+.

Despite the many simplifying assumptions (rank-1 approximation, broadband forcing, two-step procedure), the model is able to capture the trends observed in DNS reasonably well. In particular, the model successfully predicts the emergence of structures that are long in the spanwise direction, and contribute substantially to the premultiplied spectrum for wall-normal velocity, $\kappa_x\kappa_z E_{vv}$ (middle panel). Garcia-Mayoral & Jimenez (2011) attribute the emergence of these spanwise structures to a Kelvin-Helmholtz type of mechanism, and suggest that these structures are primarily responsible for the breakdown of the viscous regime within the riblet grooves. Another interesting feature captured by the model is the enhanced amplification of structures with spanwise wavelength shorter than the spacing s^+ in the spectra for wall-normal velocity and Reynolds' stress. Finally, the model also predicts relatively minor changes to $\kappa_x\kappa_z E_{uu}$ compared to the smooth-wall case, which is consistent with the DNS.

Of course, there are some important quantitative differences. For instance, the spanwise structures observed in DNS have wavelength $\lambda_x^+ \approx 150$, while the model predicts that structures with $\lambda_x^+ \approx 80$ are most energetic. This is consistent with the simplified instability analysis pursued by Garcia-Mayoral & Jimenez (2011), which also suggests that structures with spanwise wavelength $\lambda_x^+ < 100$ have the highest growth rates. In general, for both the riblet and smooth wall predictions, the model is biased towards smaller wavelengths compared to the DNS. This could potentially be attributed to the broadband forcing assumption. In the real flow, there is unlikely to be significant nonlinear forcing at smaller length scales, particularly close to the wall.

Figure 3 compares a snapshot from DNS with predictions that include velocity contributions from just two rank-1 modes, corresponding to the near-wall cycle and the Kelvin-Helmholtz type structures that emerge over riblets. Specifically, this figure superposes contributions from resolvent modes with nominal wavenumber-frequency combinations $(\lambda_x^+, \lambda_z^+, c^+) = (10^3, 10^2, 10)$ and $(\lambda_x^+, \lambda_z^+, c^+) = (150, 840, 6)$, along with the coupled harmonics introduced by spanwise variations in mean velocity and permeability. The inset in Fig. 3a confirms that volume penalization successfully drives the velocity to zero within the solid domain (*n.b.* all vectors have been plotted). For this combination of modes, the no-slip boundary condition at the riblet surfaces is enforced to $O(10^{-3})$ and the predicted velocities within the solid domain are even smaller. The two modes qualitatively reproduce many flow features from DNS, including regions of alternating positive and negative velocity with spanwise length scale corresponding to the riblet spacing, intermittent bursts of high activity, evidence of meandering, and extended regions of spanwise and streamwise coherence. In addition, the counter-rotating vortices associated with the near-wall cycle are pushed up above the riblets.

Homogeneous Porous Medium

As further evidence of the predictive capability of the modified resolvent framework, Fig. 4 compares model predictions with DNS results for turbulent flow in a channel that is partially filled with a homogeneous porous medium (Breugem *et al.*, 2006). Model predictions for the premultiplied spectra of streamwise and wall-normal velocity, shown in Fig. 4a-b, suggest that the flow at the porous interface is dominated by structures with large spanwise length scales, $\lambda_z/h > 1$, and relatively low aspect ratios, $\lambda_x \approx \lambda_z$ (shaded contours). In contrast, the streamwise velocity spectrum near the top, smooth wall is dominated by longer structures with limited spanwise extent ($\lambda_x \approx 2h$ and $\lambda_z \approx 0.2h$; solid lines). Note that these predicted spectra once again invoke the broadband forcing assumption.

Importantly, these spectral predictions also help identify resol-

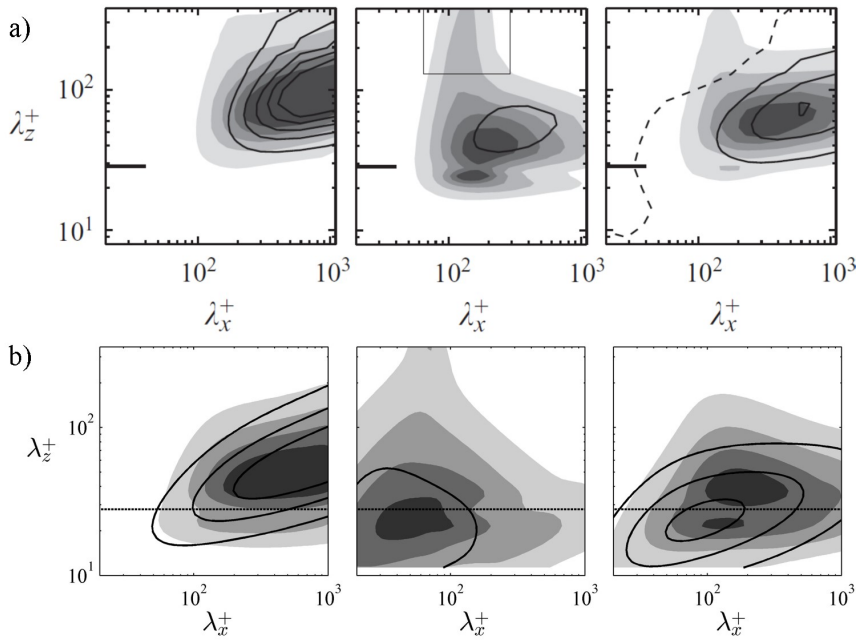

Figure 2. Spectral predictions for riblets. (a) From left to right: premultiplied spectra for u^2, v^2 and Reynolds' stress at $y^+ \approx 5$ from DNS by Garcia-Mayoral & Jimenez (2011) over rectangular riblets with spacing $s^+ = 28$ at $Re_\tau = 180$. Note that $y^+ = 0$ corresponds to the tips of the rectangular riblets. The superimposed solid contours show the smooth-wall case. (b) Corresponding premultiplied spectra predicted by resolvent model, assuming broadband forcing. The dashed horizontal line represents the riblet spacing. The solid contours again show predictions for the smooth-wall case.

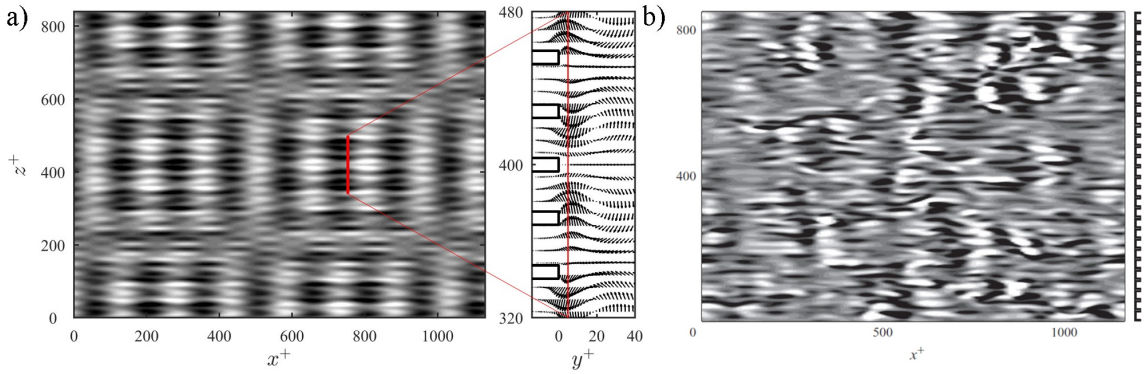

Figure 3. Predicted flow structure over riblets. (a) Resolvent-based predictions of wall-normal velocity at $y^+ \approx 5$ over riblets with spacing $s^+ = 28$ at $Re_\tau = 180$. These predictions were obtained by combining just two modes, characterized by length and velocity scales $(\lambda_x^+, \lambda_z^+, c^+) = (10^3, 10^2, 10)$ and $(\lambda_x^+, \lambda_z^+, c^+) = (150, 840, 6)$. Black shading represents negative velocity and white shading represents positive velocity. (b) Snapshot from DNS for identical riblet geometry and Reynolds number (Garcia-Mayoral & Jimenez, 2011).

vent modes can serve as representative models for dynamically-important flow features. The flow field for a resolvent mode that is highly energetic at the top wall is shown in Fig. 4d, while the flow field for the mode that contributes the most to the wall-normal velocity at the porous interface is shown in Fig. 4e. These modes correspond to the wavenumber combinations highlighted in Fig. 4a and Fig. 4b, respectively. Consistent with the DNS snapshot shown in Fig. 4c, the resolvent mode energetic at the smooth wall has alternating regions of high- and low- streamwise velocity with a slightly inclined shear layer separating the two. This mode features counter-rotating vortices in the spanwise-wall normal plane (not shown here), and is structurally similar to the dynamically important near-wall cycle (Robinson, 1991; Waleffe, 1997; Schoppa & Hussain, 2002). In contrast, the resolvent mode that is most energetic at the porous interface shows the presence of taller vortices that penetrate well into the porous medium ($y < 0$) and generate counter-rotating spanwise rollers in the fluid domain. The length scale of this interfacial structure and the predicted flow field both bear strong resemblance to the DNS observations. This interfacial structure once again resembles Kelvin-Helmholtz type vortices that are known to appear in flows over vegetation canopies and porous media.

DISCUSSION

The preliminary results presented in this paper suggest that the volume-averaged Navier-Stokes equations provide a useful

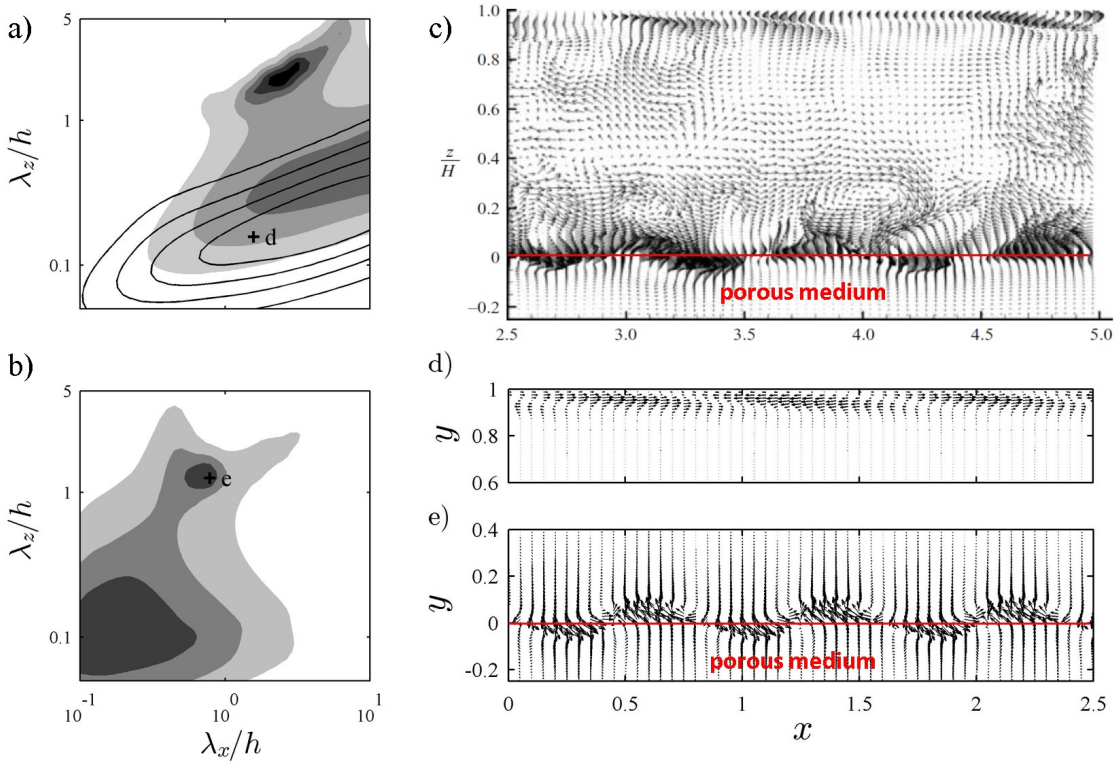

Figure 4. Predictions for porous medium. (a) Shaded contours showing model predictions for the premultipled spectrum of streamwise velocity, $\kappa_x\kappa_z E_{uu}$, at the porous interface. The solid contours show model predictions near the top, smooth wall. (b) Model predictions for the premultiplied spectrum of wall-normal velocity, $\kappa_x\kappa_z E_{vv}$, at the porous interface. (c) Snapshot of turbulent flow field over permeable medium from DNS by Breugem *et al.* (2006). (d,e) Predicted flow fields for the most amplified resolvent modes at the wavenumber combinations identified in highlighted in plots (a) and (b), respectively.

framework for the development of low-order models based on resolvent analysis for turbulent flows over porous and patterned walls. Volume-averaging is standard in the study of porous media flows, while volume-penalization allows for useful approximation of spatially-varying surface features.

Keep in mind that volume-penalization does have two important limitations when it comes to modeling surface features. First, the boundary conditions will not be satisfied exactly. Second, volume penalization is likely to work best for periodic or regular surfaces with limited spectral content, such that the coupled problem involving multiple Fourier harmonics remains computationally tractable. While the first limitation precludes accurate prediction of quantities like local wall shear stress, it still allows for the development of wall models that link spectral features of the surface with those of the flow. The second limitation makes the modeling of irregular, rough surfaces challenging. However, recent successes in the development of low-order representations of rough surfaces via proper orthogonal decomposition (Mejia-Alvarez & Christensen, 2010) suggest that retaining a small number of Fourier harmonics could still yield useful results.

Moving forward, the framework developed here will be used to (i) evaluate the effect of streamwise-constant riblets with varying shape and size, and (ii) to consider how the large-scale structures identified in flows over porous media scale with the Reynolds number and Darcy number.

ACKNOWLEDGMENTS

This work was supported by the Air Force Office of Scientific Research under AFOSR grant No. FA9550-17-1-0142 (Program Manager: Dr. Douglas Smith). The author is grateful to Dr. Breugem for providing DNS data for partially-porous turbulent channel flow.

REFERENCES

Angot, Philippe, Bruneau, Charles-Henri & Fabrie, Pierre 1999 A penalization method to take into account obstacles in incompressible viscous flows. *Numerische Mathematik* **81** (4), 497–520.

Breugem, WP, Boersma, BJ & Uittenbogaard, RE 2006 The influence of wall permeability on turbulent channel flow. *Journal of Fluid Mechanics* **562**, 35–72.

García-Mayoral, R. & Jiménez, J. 2011 Drag reduction by riblets. *Philosophical Transactions of the Royal Society of London A: Mathematical, Physical and Engineering Sciences* **369** (1940), 1412–1427.

Garcia-Mayoral, Ricardo & Jimenez, Javier 2011 Hydrodynamic stability and breakdown of the viscous regime over riblets. *Journal of Fluid Mechanics* **678**, 317–347.

Ghisalberti, M. 2009 Obstructed shear flows: similarities across systems and scales. *Journal of Fluid Mechanics* **641**, 51–61.

Khadra, Khodor, Angot, Philippe, Parneix, Sacha & Caltagirone, Jean-Paul 2000 Fictitious domain approach for numerical modelling of navier–stokes equations. *International journal for numerical methods in fluids* **34** (8), 651–684.

Luhar, M., Sharma, A. S. & McKeon, B. J. 2014*a* On the structure and origin of pressure fluctuations in wall turbulence: predictions based on the resolvent analysis. *Journal of Fluid Mechanics* **751**, 38–70.

Luhar, M., Sharma, A. S. & McKeon, B. J. 2014*b* Opposition con-

trol within the resolvent analysis framework. *Journal of Fluid Mechanics* **749**, 597–626.

Luhar, M., Sharma, A. S. & McKeon, B. J. 2015 A framework for studying the effect of compliant surfaces on wall turbulence. *Journal of Fluid Mechanics* **768**, 415–441.

McKeon, B. J. & Sharma, A. S. 2010 A critical-layer framework for turbulent pipe flow. *Journal of Fluid Mechanics* **658**, 336–382.

Mejia-Alvarez, R & Christensen, KT 2010 Low-order representations of irregular surface roughness and their impact on a turbulent boundary layer. *Physics of Fluids (1994-present)* **22** (1), 015106.

Moarref, Rashad, Sharma, Ati S, Tropp, Joel A & McKeon, Beverley J 2013 Model-based scaling of the streamwise energy density in high-Reynolds number turbulent channels. *Journal of Fluid Mechanics* **734**, 275.

Ochoa-Tapia, J. A. & Whitaker, S. 1995*a* Momentum transfer at the boundary between a porous medium and a homogeneous fluidi. theoretical development. *International Journal of Heat and Mass Transfer* **38** (14), 2635–2646.

Ochoa-Tapia, J. A. & Whitaker, S. 1995*b* Momentum transfer at the boundary between a porous medium and a homogeneous fluidii. comparison with experiment. *International Journal of Heat and Mass Transfer* **38** (14), 2647–2655.

Reynolds, W. C. & Tiederman, W. G. 1967 Stability of turbulent channel flow with application to Malkus's theory. *Journal of Fluid Mechanics* **27**, 253–272.

Robinson, S. K. 1991 Coherent motions in the turbulent boundary-layer. *Annual Review of Fluid Mechanics* **23**, 601–639.

Schoppa, W. & Hussain, F. 2002 Coherent structure generation in near-wall turbulence. *Journal of Fluid Mechanics* **453**, 57–108.

Sharma, A. S. & McKeon, B. J. 2013 On coherent structure in wall turbulence. *Journal of Fluid Mechanics* **728**, 196–238.

Waleffe, F. 1997 On a self-sustaining process in shear flows. *Physics of Fluids* **9** (4), 883–900.